SPEED-SENSORLESS CONTROL STRATEGY FOR MULTI-PHASE INDUCTION GENERATOR IN WIND ENERGY CONVERSION SYSTEMS

by

Boris P. DUMNIĆ*[*], Dragan M. MILIĆEVIĆ, Bane P. POPADIĆ, Vladimir A. KATIĆ, and Zoltan J. ČORBA

Faculty of Technical Sciences, University of Novi Sad, Novi Sad, Serbia

Original scientific paper
DOI:10.2298/TSCI151019032D

Renewable energy sources, especially wind energy conversion systems (WECS), exhibit constant growth. Increase in power and installed capacity has led to advances in WECS topologies. Multi-phase approach presents a new development direction with several key advantages over three-phase systems. Paired with a sensorless control strategy, multi-phase machines are expected to take primacy over standard solutions. This paper presents speed sensorless vector control of an asymmetrical six-phase induction generator based on a model reference adaptive system. Suggested topology and developed control algorithm show that sensorless control can yield appropriate dynamic characteristics for the use in WECS with increase in reliability and robustness.

Key words: *wind energy, multi-phase machine, vector control, speed estimation*

Introduction

Recently, relevant reports show that cumulative power of installed wind energy conversion systems (WECS) worldwide was over 360 GW at the end of 2014 [1]. The annual growth in capacity, during the year 2014, was an astonishing 44%, with the record breaking annual installed capacity over 50 GW. Most dominant increase was exhibited by China with 23 GW, or 45% of world annual market. Future of wind energy market looks bright, with forecast showing the trend of stabilization after 2015 and expected annual market growth at 4-6% before 2019. The trend would set the cumulative capacity growth between 11% and 15%, potentially ending 2019 at global cumulative installed capacity just about 650 GW, as seen in fig. 1 [1].

High penetration of renewable energy sources, especially WECS, has led to the introduction of new technologies and solutions in order to deal with known deficiencies of traditional systems [2, 3]. Currently deployed WECS topologies have achieved their limit, especially with respect to their power rating. Mostly bound by the advances in power electronic converters, there are several approaches in overcoming these constraints [4, 5]. Two major directions in further development of WECS are: multi-winding (multi-phase) generators with distributed converters and multiple generators with distributed gearbox. Clear disadvantage of the latter topology lies in the complex gearbox system, which can significantly increase the

[*] Corresponding author; e-mail: dumnic@uns.ac.rs

price, and maintenance cost of the system. Furthermore, complex gearbox system can lead to severe decrease in WECS reliability.

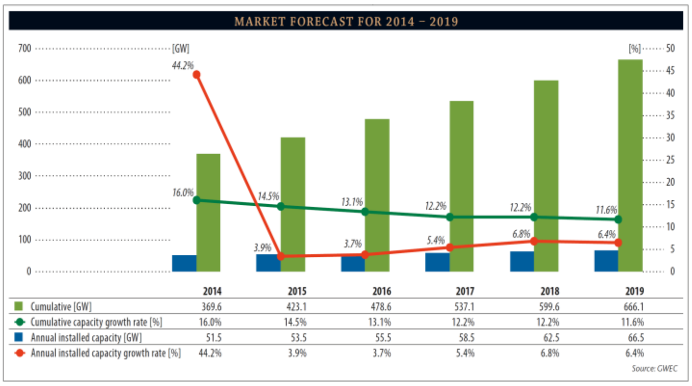

Figure 1. Wind energy market statistic 2014-2019 (source GWEC)

On the other hand, using multi-phase generators in WECS offer several advantages in addition to increasing the power rating of the system. In the midst of multiphase machine types one concept claimed its place as one of the most interesting and most investigated. Those are asymmetrical six-phase (dual three-phase) induction machines that have two three-phase winding sets with spatial shift of 30 electrical degrees [6, 7]. Multi-phase drives, with six-phase induction machines, are featured in highly reliable applications, making them a perfect fit in wind energy applications. With the standard benefits that induction machine offers, introduction of multiple phases allows the drive to become prominently immune to failure. Unlike their three-phase counterparts, six-phase machines in WECS can operate under faulty conditions by a simple reduction to a system with lower phase number. As a result, the robustness and reliability of the drive is greatly increased [8].

However, mathematical model of the six-phase machine operating with at least one phase fault is different from mathematical model of a machine operating in a regime without faults. The complete analysis and modelling of a six-phase machine under phase fault is presented in [9]. This change in mathematical model inevitably leads to the change in control algorithm, modulation technique and speed estimation algorithm. Literature proposes several different techniques for six-phase machine operation under faulty conditions. One solution recommends disconnection of a three-phase winding containing the faulty phase [10, 11]. The second solution proposes the reduction of the machine phase number to include all healthy phases, with the possibility of achieving the rated machine torque [12], while the third common solution proposes the stator current limitation at rated value, in addition to the phase number reduction. Since the change in mathematical model is significant and implies the change in control algorithm and all estimators, this analysis exceeds the intended scope of this paper and will not be further discussed.

Compared to the three-phase solutions, six-phase machine offers a variety of control options, regarding operating regimes with wind power lower than nominal, with the possibility of maintenance cost reduction by applying suitable optimization and selecting appropriate number of phases for power transfer. Moreover, using six-phase machine in WECS will lessen the mechanical stress of the system components since they have significantly lower torque ripple [6]. With the increase in efficiency, by proper control of the machine side converter, the WECS based on a six-phase induction machine makes for a robust, relatively inexpensive and highly reliable solution.

Considering main advantages of such a drive, the extension of the field oriented control (FOC) principle from three-phase to six-phase machines offers well-known, robust and computationally non-demanding algorithm [13]. However, proper implementation of the vector control algorithm requires accurate rotor speed signal, in order to provide the decoupling between machine torque and flux. More often, acquiring such signals can have negative impact on the system robustness and reliability. This is particularly emphasized by the harsh environmental and WECS operating conditions. Reliability of the WECS can, therefore, be improved by eliminating the speed sensor, whilst reducing maintenance cost.

Elimination of the speed sensor is possible with the use of six-phase induction generator states and outputs estimation algorithm. Model reference adaptive system (MRAS) speed estimation algorithm provides simple and reliable technique, with dynamic performances similar to those of standard drives that include speed measurement [14]. The introduction of speed estimation technique based on MRAS algorithm to the six-phase induction machine drive will greatly complement positive features of the overall system. Furthermore, known MRAS insufficiencies can be surpassed by the same improvements established for standard three-phase induction machine drives [15, 16].

This paper will present the speed sensorless vector control of an asymmetrical six-phase induction machine. Speed estimation technique is based on a MRAS algorithm adjusted for the use in asymmetrical six-phase induction machine. Simulation results will show that the speed estimation method is capable of tracking the rotational speed of the machine under realistic conditions. Proposed technique is computationally very efficient and easy to implement, which in addition to its robustness makes it suitable for implementation in WECS.

Overview of the system topology and control strategy

Asymmetrical six-phase induction generator with full-capacity converter

With the constant reduction in prices of semiconductors, and constant advances in technology, market is opened for new reliable converter topologies to be used in WECS. Alongside the advances in power electronics, and in regard to the power limitations of the current WECS topologies, solutions with different electrical machines can be offered now. The benefits offered by multi-phase machines can simply be transferred to WECS, when it is possible to adequately implement the control using multi-phase converters [17].

A WECS topology directly derived from its three-phase counterpart is the topology with asymmetrical six-phase induction generator with full-capacity converter, shown in fig. 2. This topology consists of six-phase squirrel cage induction generator (SCIG) and back to back two-level voltage source converters (VSC), with a six-phase machine side and a three-phase grid side converter. Both VSC use insulated-gate bipolar transistors (IGBT) as basic switching components; they have standard bridge topology and are coupled using the DC-link. Using this topology enables surpassing power limitation of standard WECS topologies, while the power limitation of the converter is surpassed with parallelizing several three-phase VSC channels [3].

To implement maximum power point tracking (MPPT) algorithms, the generator side converter (voltage source rectifier – VSR) is used to control machine speed and/or torque. Power transfer is completed with grid side converter (voltage source inverter – VSI), controlling the DC-link voltage and injected active and/or reactive power. This allows for fully independent operation of six-phase SCIG in full speed range, while VSI fulfils all the necessary requirements regarding grid synchronization.

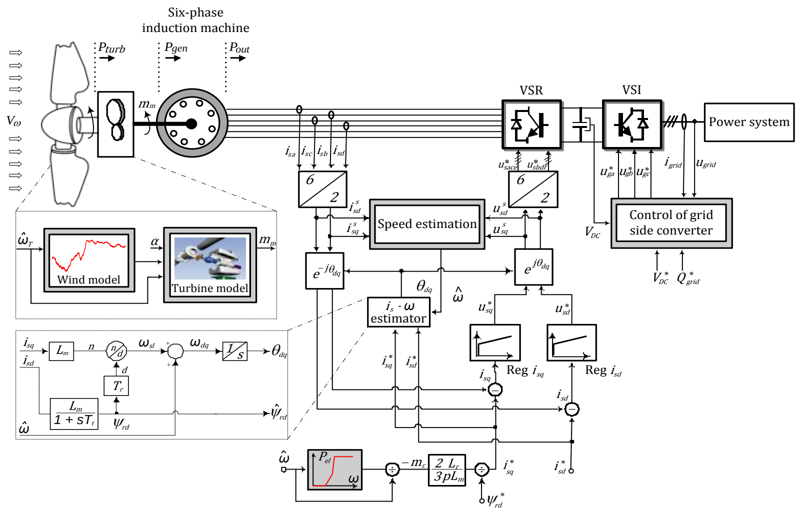

Figure 2. Variable speed WECS with six-phase SCIG and full-capacity power converter

Since the focus of this paper is speed-sensorless vector control of six-phase SCIG, control of grid side converter is performed using standard control techniques and those will not be discussed in detail. The machine side converter is controlled using well known indirect field oriented control (IFOC), beneficial for operation in four-quadrant down to standstill [18-21].

Machine model and modulation strategy

Mathematical representation of the asymmetrical six-phase induction machine used in the paper is based on voltage space decomposition (VSD) theory [22, 23]. With the application of the amplitude invariant VSD transformation matrix, stator and rotor equations from the original domain (a, b, c, x, y, z), are transferred to three two-dimensional orthogonal (decoupled) subspaces (α, β, μ_1, μ_2, z_1, z_2). The fundamental components are contained in α-β subspace as shown in eq. (1), while the other subspace, designated by μ_1-μ_2 in eq. (2), contains the loss producing components. The third, z_1-z_2 subspace containing zero-sequence components, equal to zero in regard to the particular topology, is not presented in this paper.

$$\begin{bmatrix} u_{\alpha s} \\ u_{\beta s} \\ 0 \\ 0 \end{bmatrix} = \begin{bmatrix} R_s + \left(L_{ls} + M\right)\cdot \mathrm{d/dt} & 0 & M\cdot \mathrm{d/dt} & 0 \\ 0 & R_s + \left(L_{ls} + M\right)\cdot \mathrm{d/dt} & 0 & M\cdot \mathrm{d/dt} \\ M\cdot \mathrm{d/dt} & \omega_r \cdot M & R_r^{'} + \left(L_{lr}^{'} + M\right)\cdot \mathrm{d/dt} & \omega_r \cdot \left(L_{lr}^{'} + M\right) \\ -\omega_r \cdot M & M\cdot \mathrm{d/dt} & -\omega_r \cdot \left(L_{lr}^{'} + M\right) & R_r^{'} + \left(L_{lr}^{'} + M\right)\cdot \mathrm{d/dt} \end{bmatrix} \cdot \begin{bmatrix} i_{\alpha s} \\ i_{\beta s} \\ i_{\alpha r} \\ i_{\beta r} \end{bmatrix} \tag{1}$$

$$\begin{bmatrix} u_{\mu_1 s} \\ u_{\mu_2 s} \\ 0 \\ 0 \end{bmatrix} = \begin{bmatrix} R_s + L_{ls}\cdot \mathrm{d/dt} & 0 & 0 & 0 \\ 0 & R_s + L_{ls}\cdot \mathrm{d/dt} & 0 & 0 \\ 0 & 0 & R_r + L_{lr}\cdot \mathrm{d/dt} & 0 \\ 0 & 0 & 0 & R_r + L_{lr}\cdot \mathrm{d/dt} \end{bmatrix} \cdot \begin{bmatrix} i_{\mu_1 s} \\ i_{\mu_2 s} \\ i_{\mu_1 r} \\ i_{\mu_2 r} \end{bmatrix} \tag{2}$$

The machine torque in stationary reference frame can be acquired by:

$$T_e = 3 \cdot \frac{P}{2} \cdot \frac{M}{L_r}\left(\psi_{\alpha r} \cdot i_{\beta s} - \psi_{\beta r} \cdot i_{\alpha s}\right) \tag{3}$$

Mathematical model after transformation to the synchronous rotating reference frame is identical to the three-phase machine as it is presented in [7].

The control of the machine side converter is made according to the novel space vector selection scheme presented in [7]. The main advantage of this technique in comparison with standard techniques is excellent mitigation of components in μ_1-μ_2 subspace and utilization of the DC-link, while significantly simplifying implementation [24]. For reference vector approximation, selection scheme uses three large vectors and one middle size vector. In order to achieve these vectors approximation, pulse-width modulation (PWM) technique, described in [7], varies channel active high/active low logic during transitions over certain sectors. However, it is shown in [24] that this can be achieved with PWM module of a commercially available digital signal processor (DSP).

Speed estimation algorithm for six-phase SCIG

The WECS environment during operation usually consists of severe and harsh conditions with wide temperature and wind speeds ranges, heavy torques, vibration and frequently even chemically aggressive environments (off-shore installations). Consequently, elimination of speed sensor improves system robustness with the added benefit of significant reduction in regular and emergency maintenance cost. On the other hand, information on the rotational speed of generator is necessary for precise IFOC control. This has led to numerous techniques for rotor speed estimation to be developed [14-16, 25]. Based solely on machine currents and voltages measurement these techniques are used for speed estimation in shaft-sensorless drives. The most popular method for rotor speed estimation is derived using MRAS [14].

Estimation algorithm based on MRAS uses closed loop control system and can, therefore, be referred to as an observer. Three main components of the MRAS observer are reference model, adaptive model and adaptation mechanism, as shown in fig. 3. Both models are mathematical representation of the machine that reflects current machine states. Reference model fails to feature value estimated by MRAS observer, *i. e.* rotor speed. Insight in the desired value (rotational speed) is provided by the adaptive model, since the mathematical representation contains estimated value of MRAS observer. According to a predefined function, adaptive model aligns estimation to the actual speed value, exploiting the difference between relevant values in reference and adaptive models. Common name for the reference model is voltage estimator, whereas adaptive model is referred to as current estimator. Classification of MRAS techniques is made in accordance to the selected value for comparison. Mostly, stator flux, rotor flux, back electromotive force (EMF), active and reactive power are used [14]. Paper suggests MRAS observer based on comparison of the rotor flux, achieved using machine voltage equations for stator and rotor windings.

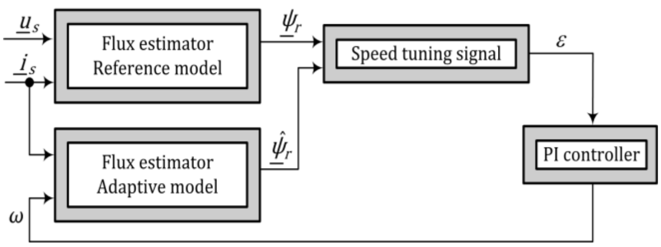

Figure 3. The MRAS based rotor speed observer.

Reference model estimator can be represented using eq. (4). As it can be noted, this estimator uses stator voltages and currents in order to calculate rotor flux linkage components ($\Psi_{\rm rd}$, $\Psi_{\rm rq}$). Chosen reference frame is indicated by the superscript (s) in these equations, and considering the machine used (SCIG), stationary reference frame was chosen. In the equation L'_s represents the stator transient inductance.

$$\psi_{rd}^{s} = L_r \big/ M \left[\int \left(u_{sd}^{s} - R_s i_{sd}^{s} \right) \mathrm{d}t - L'_s \, i_{sd}^{s} \right]$$
$$\psi_{rq}^{s} = L_r \big/ M \left[\int \left(u_{sq}^{s} - R_s i_{sq}^{s} \right) \mathrm{d}t - L'_s \, i_{sq}^{s} \right] \tag{4}$$

Voltage equations in stationary reference frame are used for the adaptive model estimator shown in eq. (5). This model uses stator currents and speed signal for calculation of rotor flux linkage components. Estimated quantities are denoted using symbol ^ in the following equations:

$$\hat{\psi}_{rd}^{s} = 1 \big/ T_r \int \left(M i_{sd}^{s} - \hat{\psi}_{rd}^{s} - \hat{\omega} T_r \hat{\psi}_{rq}^{s} \right) \mathrm{d}t$$
$$\hat{\psi}_{rq}^{s} = 1 \big/ T_r \int \left(M i_{sq}^{s} - \hat{\psi}_{rq}^{s} + \hat{\omega} T_r \hat{\psi}_{rd}^{s} \right) \mathrm{d}t \tag{5}$$

Adaptation mechanism is based on proportional-integral (PI) controller type and is represented by $\hat{\omega} = (K_p + K_i/s) \cdot \varepsilon$, where $\varepsilon = \hat{\Psi}_{rd}^{s} \Psi_{rq}^{s} - \Psi_{rd}^{s} \hat{\Psi}_{rq}^{s}$. This mechanism is used to align the estimated and actual value of the speed. Error value, as evident, is proportional to the sine value of angle difference between output vectors of reference and adaptive models. Integral gain in adaptation mechanism will ensure that steady state value of ε is equal to zero.

The paper proposes using described MRAS algorithm for speed estimation with six-phase SCIG topology for WECS, enhancing the robustness and reliability of the system. Transfer to the six-phase system, from well established three-phase MRAS speed estimation, is made using simple extension principle. On the other hand, caused by the severe environmental conditions, thermal drift can easily make the machine resistances vary up to ±20% in comparison with estimator predefined values. In that regard, MRAS observer with detuned parameters (stator and rotor resistance) can be observed as an encoder with an inherent ripple, consequently leading to oscillations and instability of the WECS drive. Aside from the influence on dynamic performance MRAS observer parameter detuning will lead to speed estimation error in steady state [14]. Speed estimation error in steady state will also lead to power losses due to inaccurate speed value supplied to the MPPT algorithm, faulty operation of pitch angle regulation system and faulty operation of other control algorithms (*e. g.* power limitation) that use machine speed as a control variable. In order to deal with these well-known insufficiencies, the improved MRAS techniques can be implemented applying the same extension principle [15, 16, 26].

Verification of theoretical principles

The proposed theoretical consideration of applying known sensorless control principles to a six-phase SCIG used in WECS are verified using Matlab/Simulink model of the system. Basis for the model is represented in fig. 2., while the simulation results will show the successful implementation of MRAS speed estimation and decoupled vector control for six-phase induction machine. Separate stages, with different sampling times, for current and speed control are set in the simulation.

Speed estimation technique is verified using speed closed control loop for the six-phase machine with IFOC principles implemented. The flux was set to the nominal value, and the machine was first accelerated to the reference speed of 40 rad/s, while the load torque was kept at zero. When the machine achieved steady state, the load torque of 10 Nm was applied at the time 0.8 second. The machine torque was kept through the speed reference change, after which, at time 1.4 second the torque was set to zero again. In fig. 4. six-phase machine actual and estimated speed is presented, where the obvious transitions of torque and speed can be noted. In addition, the estimated and actual speed match almost perfectly providing the strong ground for practical speed sensorless drive implementation. High precision of speed estimation will ensure decoupled control for IFOC strategy, aligning the synchronous rotating reference frame to the desired position.

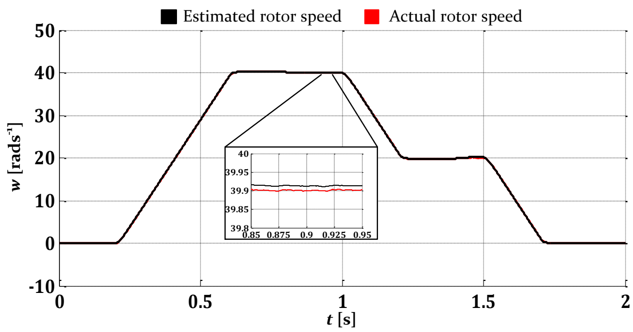

Figure 4. Machine MRAS estimated and actual rotor speed

The main principle of IFOC can be observed in d- and q-axis currents shown in fig. 5. As it can be seen, the changes in the torque producing (q-axis) current fail to influence the current in d-axis set at 0.45 A. This will lead to the constant flux for the duration of simulation. The changes in the q-axis current are fully compliant with the torque and speed transitions previously shown. Since the control of the six-phase machine is satisfactory, the currents in the stationary reference frame, shown in the fig. 6(a). are circular in shape. In addition, in fig. 6(b). the negligible loss producing components can be observed, showing the benefits offered by the novel vector selection scheme used. The novel vector selection scheme automatically neutralizes currents in μ1-μ2 plane, which increases efficiency of the system. Detailed analysis of efficiency of novel vector selection scheme, with comparison to standard modulation techniques can be found in [24].

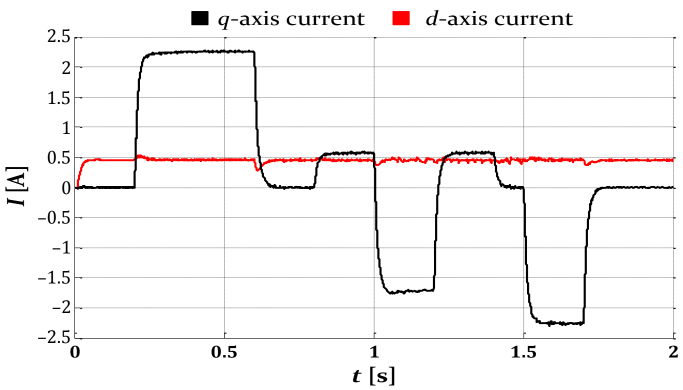

Figure 5. Flux and torque producing currents

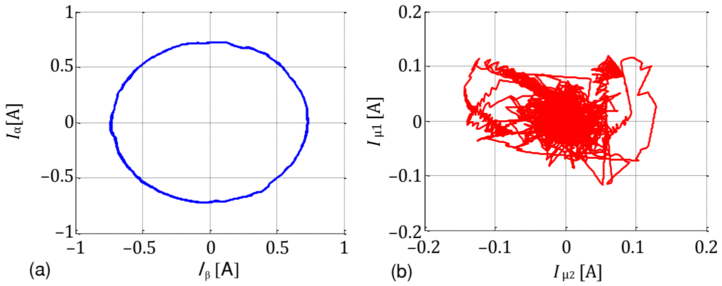

Figure 6. Current components in α-β (a) and μ1-μ2 (b) subspaces

In order to further demonstrate the behaviour of MRAS speed estimation in WECS at low wind speed, the six-phase machine was used in generator operating regime. Figure 7. shows the MRAS response during system start-up and operation under turbine torque at low wind speed. It is expected that MRAS should have poor performance at low speed and during start-up operation. However, the nature of the WECS operation allows control algorithm to easily deal with this insufficiency, since the system starts to operate only when winds speed is above the cut-in speed of the WECS. The most common induction generators operate at relatively high speeds so the effect of incorrect operation of the speed estimation scheme at low speeds is not expressed for this application. In addition, asymmetrical six-phase machine with six poles, used in this simulation and experiment, usually operates at speed ranges of 200-1100 rpm in WECS [3]. As proposed previously and demonstrated in fig. 7(b)., the torque at generator shaft is zero until the wind speed surpassed the cut-in value, at which point the speed estimation algorithm has been started. This avoids the problem with zero speed estimation and leads to high dynamic performance of MRAS speed estimation during start-up, as presented in fig. 7(a).

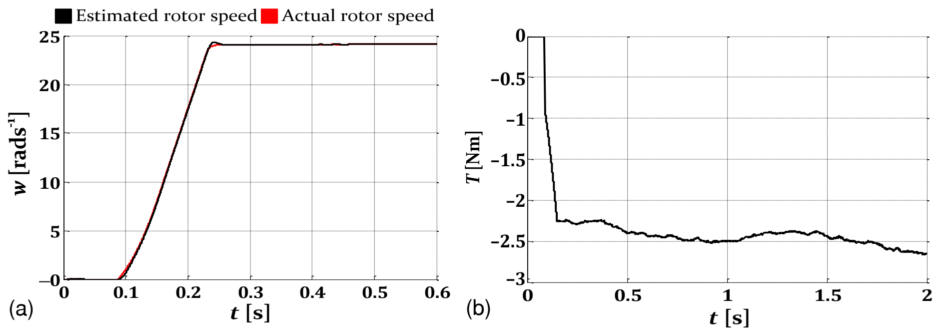

Figure 7. Speed estimation during start-up operation (a) and the turbine torque (b)

Experimental validation of the proposed WECS sensorless control scheme

Description of Laboratory WECS Prototype

Speed-sensorless control strategy for six-phase SCIG used in variable speed WECS with full-capacity converter proposed by this paper is tested and verified using advanced laboratory prototype for control of electrical drives and power electronic converters [27]. Advance research and development (R&D) station developed by authors of this paper has the possibility of running different demanding complex control strategies for multi-phase systems, standard three phase systems, grid connected converter, electrical vehicles and other [28-30]. Previously presented theory will be experimentally validated by organizing the setup to operate as a small scale WECS with asymmetrical six-phase SCIG. The physical outlook of the experimental set-up can be seen in fig. 8.

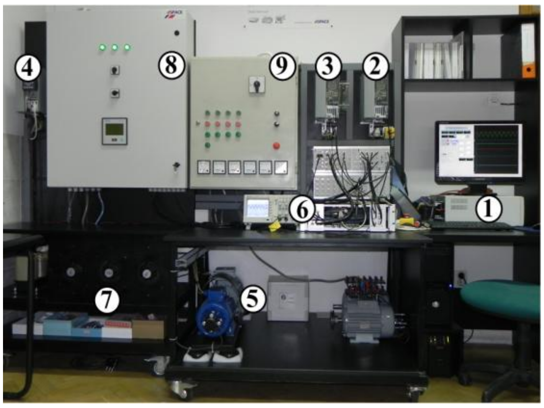

Figure 8. Small scale WECS laboratory prototype

Basic and complex control solutions are implemented using modular and highly versatile dSPACE control hardware [31]. In fig. 8. dSPACE processor board designated by 1 executes speed estimation, IFOC strategy and MPPT algorithm for the control of generator side converter designated by 2 and 3. Six-phase converter consists of two three-phase converters sharing the same DC-link which are controlled simultaneously to behave as a single unit converter. Generator side converter is coupled by DC-link with grid side converter, where standard control techniques are implemented and will not be further discussed since they are not the focus of this paper. Additionally, presentation of realistic operational conditions reference for wind turbine emulator, consisting of power converter 4 and torque controlled machine is dictated by the dSPACE system according to the actual wind data. Torque controlled machine is mechanically coupled with the six-phase SCIG and coupled group is marked by 5. Data acquisition, control signals and measured signals are routed through adapter block indicated by 6. A power transformer 7 represents the point of common coupling where generated power is supplied to the distribution network. Two distribution cabinet designated by 8 and 9 hold switching and protection gear.

Using full visual block oriented programming in Matlab/Simulink software tool real-time implementation algorithm presented in fig. 9. has been developed. Fastest subsystem, containing measurements (six-phase SCIG currents and DC-link volt-age), software system protection and PWM generation is executed at 8 kHz sampling frequency and triggered by hardware generated interrupt at the mid-point of PWM period. Current control and speed estimation subsystem is set to be executed at 4 kHz, while the MPPT algorithm was at 1 kHz; if the time constant of the WECS mechanical subsystem was significantly higher and faster control would be ineffective.

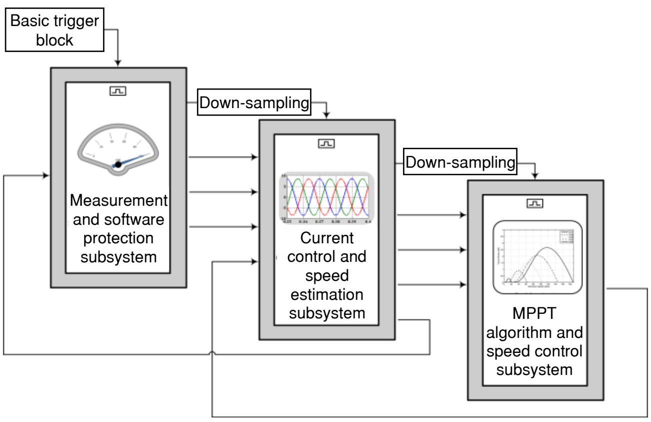

Figure 9. Structural organization of the control algorithm for real-time implementation

Experimental Results

Continuing on the principles verified by simulation, the complete small scale WECS with six-phase induction machine has been developed using previously described advanced laboratory prototype. Experimental verification is used to prove that a sensorless vector controlled six-phase SCIG could be used in the proposed WECS topology adequately.

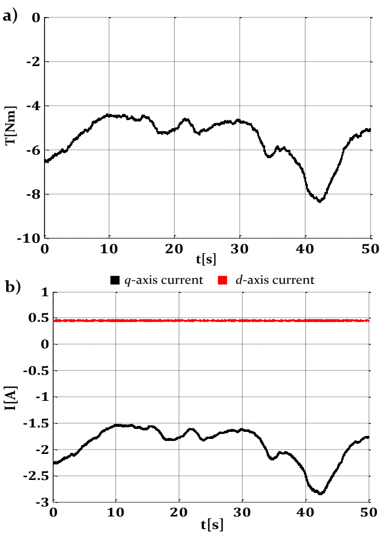

Figure 10. Emulated wind torque (a) with flux and torque producing currents (b)

For the operation of WECS based on six-phase SCIG, and according to IFOC strategy principles, the machine flux is kept at nominal value by proper control of d-axis current. The programmed MPPT algorithm, based on rotational speed estimation, generates the reference value of the torque, and consequently q-axis current. Torque reference is acquired using wind data and wind turbine model defined in Wind Turbine Blockset for Matlab/Simulink [32]. In figs. 10-13 experimental results of WECS with six-phase SCIG under variable average wind speed ranging from 10-13 m/s are given. In fig. 10, emulated wind torque at machine shaft is presented. Figure 10. also presents machine flux and torque producing currents, proving that decoupled control with constant machine flux is achieved. Observing the q-axis current, it can be easily concluded that the maximum available wind power is converted to electrical power, thus proving the adequate implementation of IFOC with MPPT. Decoupled control was made possible due to successful implementation of sensorless control and high precision of rotor speed estimation. As presented in fig. 11, estimated speed signal has high percentage match to the actual machine rotor speed. As a further proof of control quality for the proposed strategy six stator phase currents during WECS operation are sinusoidal, as observed in fig. 12. According to VSD theory and applied novel modulation strategy high efficiency control has been achieved. Verification of the former is offered by fig. 13, with negligible level of loss producing current components (μ1-μ2), and α-β components of an ideal circular shape.

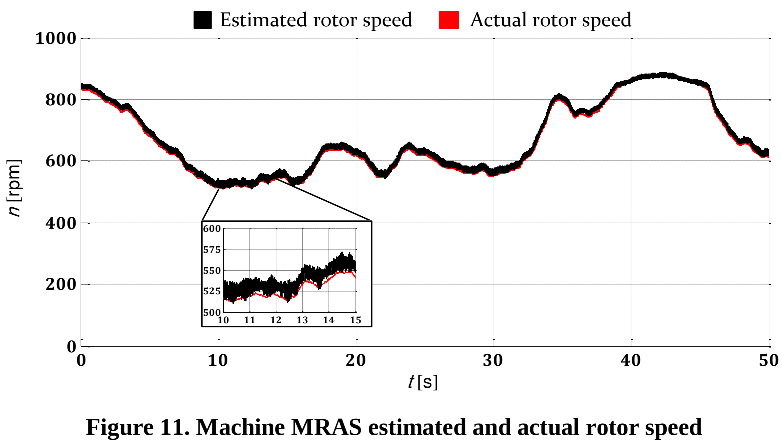

Figure 11. Machine MRAS estimated and actual rotor speed

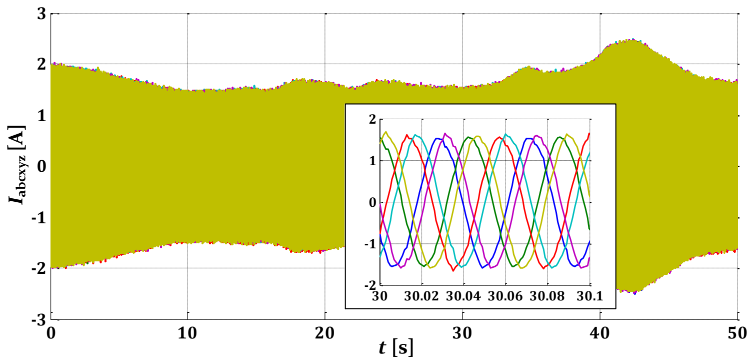

Figure 12. Stator currents in time domain

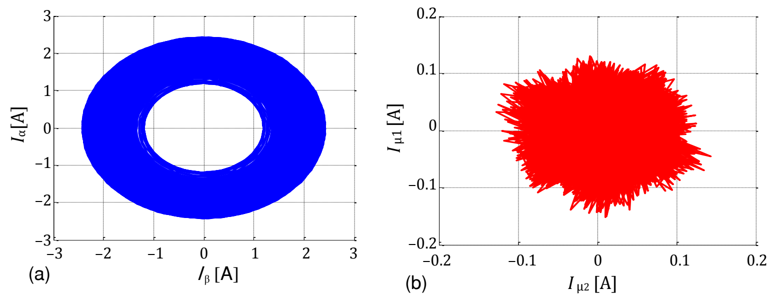

Figure 13. Current components in α-β (a) and μ_1-μ_2 (b) subspaces

Conclusions

A swift development of the technology offers the possibility of implementing novel WECS topologies with improved characteristics. This paper discusses advanced system for conversion of wind energy, equipped with six phase induction generator controlled by a speed sensorless IFOC technique. Obvious advantages over standard solutions, especially regarding the speed sensor sensitivity to environmental influences, are provided using MRAS speed estimation techniques adapted for the use with asymmetrical six-phase induction machine.

The IFOC control algorithm and precision of MRAS speed estimation has been verified using the simulation. It was proven that it is possible to achieve robust and reliable speed sensorless control, with satisfactory performance characteristics. Furthermore, a novel modulation technique allowed for the improvement of control efficiency.

After successful verification of theoretical principles, a small scale WECS prototype featuring six-phase SCIG has been developed. Using the developed prototype, the proposed topology was tested under standard wind conditions. Experimental results show that high dynamic performance of WECS with six-phase induction generator under sensorless vector control was achieved. Proposed topology significantly improves system reliability and robustness, while allowing WECS to overcome key insufficiencies of standard solutions. In addition, the total losses of the system were significantly reduced by the use of adequate modulation strategy.

With the advantages offered by multi-phase machines, and control principles shown in this paper, many of key insufficiencies of standard WECS topologies can be mitigated.

Offering strong control solutions, by a simple extension principle, will lead to fast development of novel topologies in the field. In addition, novel control strategies offered by the introduction of multi-phase machine side converters will lead to significant improvement of process efficiency.

Acknowledgment

This paper is a result of the scientific project No. III 042004 of Integrated and Interdisciplinary Research entitled *Smart Electricity Distribution Grids Based on Distribution Management System and Distributed Generation*, funded by Republic of Serbia, Ministry of Education, Science and Technological Development.

Nomenclature

i – phase current, [A]
K_p – proportional gain, [–]
K_i – integral gain, [–]
L – inductance, [H]
M – mutual inductance, [H]
P – number of pair poles, [–]
R – resistance, [Ω]
T_e – torque, [Nm]
T_r – rotor time constant, [s]
u – phase voltage, [V]

Greek symbols

ω – speed, [rads^{-1}]
Ψ – flux linkage, [Wb]
ε – error signal, [–]

Superscripts

s – stationary reference frame

Subscripts

a, b, c, x, y, z – quantities in corresponding phase
l – leakage quantities
r – stator quantities
s – stator quantities
$\alpha,\beta,\mu_1,\mu_2,d,q$ – corresponding value in adequate subspaces

Other

^ – above symbol denotes estimated value

References

[1] ***, GWEC Report, Global Wind Report – Annual Market Update 2014, Global Wind Energy Council, 2014
[2] Patil, N. S., Bhosle, Y. N., A Review on Wind Turbine Generator Topologies, *International Conference on Power, Energy and Control (ICPEC)*, Dindigul, Tamil Nadu, India, 2013, pp. 625-629
[3] Wu, B., *et al.*, *Power Conversion and Control of Wind Energy Systems*, John Wiley and Sons, IEEE Press, USA, 2011
[4] Md Rabiul, I., *et al.*, *Power Converters for Wind Turbines: Current and Future Development*, Materials and Processes for Energy: Communicating Current Research and Technological Developments, FORMATEX, pp. 559-571, 2013
[5] Blaabjerg, F., *et al.*, Future on Power Electronics for Wind Turbine Systems, *The Institution of Engineering Technology, IET, Electric Power Applications, EPA, 1* (2007), 4, pp. 489-516
[6] Levi, E., *et al.*, Multiphase Induction Motor Drives - A Technology Status Review, *IEEE Journal of Emerging and Selected Topics in Power Electronics, 1* (2013), 3, pp. 139-152
[7] Milićević, D., *et al.*, New Space Vector Selection Scheme for VSI Supplied Dual Three-Phase Induction Machine, *Advances in Electrical and Computer Engineering, 13* (2013), 1, pp. 59-64
[8] Parsa, L., On Advantages of Multi-Phase Machines, *Industrial Electronics Society, 2005. 31st Annual Conference of IEEE* , IECON 2005., Sheraton Capital Center Raleigh, N.C., USA, 2005
[9] Zhao, Y., Lipo, T. A., Modeling and Control of a Multi-Phase Induction Machine With Structural Unbalance Part I, *IEEE Transaction on Industrial Electronics, 11* (1996), 3, pp. 570-577
[10] Mantero Paola, E., Marina, G., An Optimized Control Strategy for Double Star Motors Configuration in Redundancy Operation Mode, *Proceedings*, European Power Electronics and Applications Conference EPE, Lausanne, Switzerland, 1999
[11] Golubev, A. N., Ignatenko, S. V., Anomalous Operation of Multiphase Asynchronous Electric Drive, *Russian Electrical Engineering, 72* (2001), 10, pp. 22-28

[12] Levi, E., Multiphase Electric Machines for Variable-Speed Applications, *IEEE Transaction on Industrial Electronics*, *55* (2008), 5, pp. 1893-1909
[13] Bojoi, R., *et al.*, Dual-Three Phase Induction Machine Drives Control-A Survey, *IEEJ Transaction on Industry Application*, *126* (2006), 4, pp. 420-429
[14] Vas, P., *Sensorless Vector and Direct Torque Control*, Oxford Univ. Press, NY, 1998, ch. 4
[15] Vas, P., *Artificial-Intelligence-Based Electrical Machines and Drives: Application of Fuzzy, Neural, Fuzzy-Neural, and Genetic-Algorithm-Based Techniques*, Oxford University Press, 1999, ch. 5
[16] Dumnić, B., *et al.*, An Improved MRAS Based Sensorless Vector Control Method for Wind Power Generator, *Journal of Applied Research and Technology – JART*, *10* (2010), 5, pp. 687-697
[17] Che, H. S., *et al.*, Current Control of a Six-Phase Induction Generator for Wind Energy Plants, *Proceedings*, 15th International Conference on Power Electronics and Motion Control, EPE/PEMC 2012, pp. LS5b.2-1-LS5b.2-7, Novi Sad, Serbia, 2012
[18] Santisteban, J. A., Stephan, R. M., Vector Control Methods for Induction Machines: An Overview, *IEEE Transactions on Education*, *44* (2001), 2, pp. 170-175
[19] Blaabjerg, F., *et al.*, Trends in Power Electronics and Control of Renewable Energy Systems, *Proceedings*, 14th International Conference on Power Electronics and Motion Control, EPE-PEMC 2010, K1-K19, Metropol Lake Resort Ohrid, Macedonia, 2010
[20] Dandil, B., Tuncer, S., Four-Quadrant Control of Multilevel Inverter Fed Induction Motor Drives, *Journal of Scientific and Industrial Research*, *67* (2008), 9, pp. 688-696
[21] Ben Slimene, M., *et al.*, Indirect Field-Oriented Control for Dual Stator Induction Motor Drive, *Proceedings*, 10th International Multi-Conference on Systems, Signals & Devices, SSD 2013, pp. 1-6, Hammamet, Tunisia, 2013
[22] Zhao, Y., Lipo, T. A., Space Vector PWM Control of Dual Three-Phase Induction Machine Using Vector Space Decomposition, *IEEE Transactions on Industry Application*, *31* (1995), 5, pp. 1100-1108
[23] Hadiouche, D., *et al.*, Space Vector PWM Techniques for Dual Three-Phase AC Machine: Analysis, Performance Evaluation and DSP Implementation, *IEEE Transactions on Industry Application*, *42* (2006), 4, pp. 1112-1122
[24] Milićević, D., *et al.*, Overview of the Six Phase VSI Control Techniques for the Dual Three-Phase Induction Machine Drive, *Proceedings*, PCIM Europe 2015; International Exhibition and Conference for Power Electronics, Intelligent Motion, Renewable Energy and Energy Management, pp. 1-8, Nuremberg, Germany, 2015
[25] Holtz, J., Sensorless Control of Induction Motor Drives, *Proceedings of the IEEE*, *90* (2002), 8, pp. 1359-1394
[26] Dumnić, B., *et al.*, Artificial Intelligence Based Vector Control of Induction Generator Without Speed Sensor for Use in Wind Energy Conversion System, *International Journal of Renewable Energy Research*,. *5* (2015), 1, pp. 299-307
[27] Dumnić, B., *et al.*, Advanced Laboratory Setup for Control of Electrical Drives as an Educational and Developmental Tool, *EUROCON*, pp. 903-909, Zagreb, 2013
[28] Adžić, E., *et al.*, Development of High-Reliability EV and HEV IM Propulsion Drive with Ultra-Low Latency HIL Environment, *IEEE Transaction on Industrial Informatics*, *9* (2013), 2, pp. 630-639
[29] Dumnić, B., *et al.*, Laboratory Test Bench for Multi-Phase Machines and Power Electronics in Electrical Vehicle Applications, *Proceedings*, 18th International Symposium on Power Electronics - Ee 2015, No. T2-8, pp. 1-5, Novi Sad, Serbia, 2015
[30] Popadić, B., *et al.*, Sophisticated Research and Development Station for Control of Grid Connected Distributed Energy Sources, *Proceedings*, X International Symposium on Industrial Electronics – INDEL 2014, pp. 210-215, Banja Luka, Republic of Srpska, B&H, 2014
[31] ***, dSpace manual, Modular Systems – Hardware Installation and Configuration Reference, dSpace gmbh, 2014
[32] Iov, F., *et al.*, *Wind Turbine Blockset in Matlab/Simulink*, UNI. PRINT Aalborg University, 2004

Paper submitted: October 19, 2015
Paper revised: November 16, 2015
Paper accepted: December 30, 2015